crystals

MDPI

*Article*

# An Effect of Boric Acid on the Structure and Luminescence of Yttrium Orthoborates Doped with Europium Synthesized by Two Different Routines

**Irena P. Kostova [1,*], Tinko A. Eftimov [2,3], Katya Hristova [1], Stefka Nachkova [1], Slava Tsoneva [1] and Alexandar Peltekov [2]**

[1] Faculty of Chemistry, Plovdiv University "Paisii Hilendarski", 24 Tsar Asen Str., 4000 Plovdiv, Bulgaria; kathhristova@gmail.com (K.H.)
[2] Photonics Research Center, Université du Québec en Outaouais, Rue 101 St-Jean Bosco, Gatineau, QC J8X 3G5, Canada
[3] Central Laboratory of Applied Physics, Bulgarian Academy of Sciences, 61 Sanct Peterburg Blvd., 4000 Plovdiv, Bulgaria
* Correspondence: irena_k87@abv.bg

**Abstract:** In this paper, we present the characteristics of photoluminescent $YBO_3$ successfully synthesized through a solid-state reaction and a microwave-assisted method. We used yttrium oxide and boric acid in excess as the starting reagents. The synthesis conditions were reflected in the fluorescent characteristics and the structure. Excess boric acid caused structural changes, as observed by the FTIR spectroscopy analysis. Powder X-ray diffraction (XRD) analysis confirmed the crystalline phases and purity of the samples. We observed improved photoluminescence properties in the samples synthesized by the microwave-assisted method. These findings enhance the understanding of the material's properties and indicate potential applications in illumination, displays, and narrow-band fluorescent smartphone-readable markers.

**Keywords:** yttrium borate; orthoborates; photoluminescence



**Citation:** Kostova, I.P.; Eftimov, T.A.; Hristova, K.; Nachkova, S.; Tsoneva, S.; Peltekov, A. An Effect of Boric Acid on the Structure and Luminescence of Yttrium Orthoborates Doped with Europium Synthesized by Two Different Routines. *Crystals* **2024**, *14*, 575. https://doi.org/10.3390/cryst14060575

Academic Editor: László Kovács

Received: 30 May 2024
Revised: 13 June 2024
Accepted: 18 June 2024
Published: 20 June 2024



## 1. Introduction

Rare earth (RE) borates are prospective materials for many fields of research and technology due to their specific properties such as catalytics, thermosensitivity, and luminescence. Their properties change depending on the RE ions, allowing possibilities for modeling excellent materials with individual characteristics suitable for different applications. RE borates have the general formula $REBO_3$ and are known as orthoborates [1]. Several polymorph modifications, including calcite, aragonite, and vaterite, can crystallize similarly to calcium carbonate. A structure known as $\pi$-$LnBO_3$, which is a pseudovaterite structure of rare earth borates, is formed from hexagonal and monoclinic structures. The crystal structure of $REBO_3$ changes depending on the size of the RE cation in the borates. Larger cations like La and Nd form an orthorhombic crystal system with a bipyramidal crystal lattice known as aragonite. Medium-sized cations like Sm to Yb and Y form a hexagonal crystal system with a dihexagonal bipyramidal lattice known as vaterite. The smallest cation, Lu, forms a hexagonal scalenohedral structure known as the calcite type at low temperatures and a vaterite-like structure above 1310 °C [2]. Adding boric acid in excess can cause changes in the crystal structure: the stoichiometric amounts of $Y_2O_3$ and boric acid are believed to result in the formulation of $YBO_3$, which is reported to have a hexagonal structure (P63/mnc) or a crystalline monoclinic cell (C2/c). Typically, the trivalent yttrium ion is coordinated by oxygen, and the structure comprises a $YO_8$ polyhedron, which is somewhat distorted from the ideal S6 point symmetry. On the other hand, boron atoms can be either three- or four-fold coordinated by oxygen, resulting in the observation

of polymorphic $YBO_3$ modifications in which either isolated trigonal $[BO_3]^{3-}$-groups or tetrahedral $[BO_4]^{3-}$-groups condensed to $[B_3O_9]^{9-}$-rings occur [1,2].

There are two theories that describe the decomposition of boric acid and its influence on crystal structure formation. Sevim et al. [3] evaluated the kinetics of the boric acid dehydration reaction assuming a two-step reaction, (1) and (2). Upon heating, orthoboric acid ($H_3BO_3$) exudes water to produce metaboric acid ($HBO_2$) in the first (1) reaction. The heating leads to the production of boron oxide ($B_2O_3$).

$$2H_3BO_3 \rightarrow 2HBO_2 + 2H_2O\uparrow \quad (1)$$

$$2HBO_2 \rightarrow B_2O_3 + H_2O\uparrow \quad (2)$$

Orthoboric acid contains basic $BO_3{}^{3-}$ structural units that are connected by hydrogen bonds in two-dimensional layers (Figure 1).

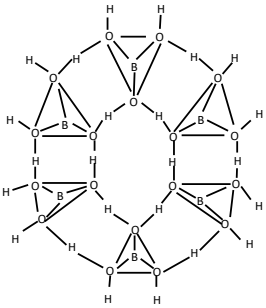

**Figure 1.** Structure of orthoboric acid.

However, while examining different crystalline structures of boric acid, Harabor et al. [4] observed three different thermally induced reaction steps (3)–(5).

$$H_3BO_3 \rightarrow HBO_2 + H_2O\uparrow \quad (3)$$

$$HBO_2 \rightarrow \frac{1}{4}H_2B_4O_7 + \frac{1}{4}H_2O\uparrow \quad (4)$$

$$\frac{1}{4}H_2B_4O_7 \rightarrow \frac{1}{2}B_2O_3 + \frac{1}{4}H_2O\uparrow \quad (5)$$

It was noted back in 1978 that a new intermediate, $H_2B_4O_7$, was formed during the decomposition of boric acid. Huber C. conducted kinetic analyses of the reaction steps and found that the decomposition of boric acid is more likely to occur in three steps rather than in two. The stoichiometric-related mass loss during the decomposition reaction is not accounted for in the often-proposed two-step reaction; thus, a three-step reaction is a more suitable description [5].

On heating, orthoboric acid partly evaporates water, and it is transformed into metaboric acid $HBO_2$. With continued heating, it forms boric oxide. The orthoboric acid content of the structural units, $BO_3{}^{3-}$, is connected with hydrogen bonds into the boroxol ring. In metaboric acid, there are long polymeric chains and ring structures, which share oxygen atoms [4].

The solid-state method is the most widely used method for obtaining polycrystalline solids from starting components in a solid aggregate state. Factors that influence the course and rate of the process include reaction conditions, structural properties of the reactants, surface area of the solids, their reactivity, and the thermodynamic free energy change associated with the reaction. The main advantages of this method are high efficiency and selectivity, uniform particle size distribution, and less environmental pollution [6].

Yttrium borate can be produced using various techniques, but the solid-state reaction method is the most commonly employed. The microwave-assisted technique is a relatively newer approach known for faster, simpler, and cost-effective processes [6]. Microwave

radiation interacts directly with the reaction components, which means that only the sample heats up, and there is no need for energy to be expended in heating furnaces, containment materials, or the sample environment. With increasing trends in the production of new materials or materials whose properties need to be optimized, a microwave-assisted method is used when conventional synthetic methods cannot be used [7,8].

Considering the other synthesis methods, such as the sol–gel method, ignition method, and combined method, we can make a comparison focusing on obtaining a product with higher purity and easy post-processing.

The sol–gel method involves the synthesis of materials through the hydrolysis of precursor salts followed by the polymerization of the resulting gel. This method ensures high purity of the products and control over the structure of the materials. However, it requires special precursor salts and involves a long process of gel drying and processing [9,10].

The combustion method effectively synthesizes ceramic materials under low-temperature conditions, involving the evaporation of precursors and subsequent thermal treatment. Despite its advantages, this method may require controlled oxidation and can lead to the formation of unwanted phases and defects. The combined methods include various techniques, such as combustion and subsequent solid-phase processing. By using these methods, it is possible to prepare materials with achieved properties. They offer a compromise between synthesis speed and control over material structure but can be more complex and involve multiple steps, leading to decreased reproducibility and yield. The specific requirements of the application and the desired properties of the materials define the choice of approach. The different methodologies have advantages and limitations that should be considered when determining a suitable method for a particular application [11]. In $YBO_3$:$Eu^{3+}$, the $Eu^{3+}$ color center produces narrow emissions at 591 nm (orange, abbreviated as O) due to magnetic dipole transition ($^5D_0$–$^7F_1$) and at 611 and 627 nm (red, abbreviated as R) due to electric dipole transition ($^5D_0$–$^7F_2$). A high R/O intensity ratio is desirable for improving the red chromaticity of $YBO_3$:$Eu^{3+}$ by optimizing experimental factors [12,13]. It was confirmed that the high-energy ball milling process reduced the particle size and improved the asymmetric ratio or color purity [14]. It was found that the addition of $H_3BO_3$ not only increases the particle size from approximately 80 nm to 1 μm, but also changes the crystal structure from cubic to hexagonal (belonging to $YBO_3$) [15,16].

Although there are extensive studies on the structure and properties of $YBO_3$ worldwide, there are still some questions regarding the reproducibility of synthesis, the dependence on synthesis conditions, and the ratio between raw materials and their impact on the characteristics of the final product. The available literature provides limited data on studies aimed at improving the purity of the red emission of $YBO_3$, which is a fundamental feature for improving its properties and expanding its applications.

The main objective of this study is to identify the structure and photoluminescent properties of yttrium borate synthesized using different procedures. We present the influence of boric acid in a wide range of excess (from 5% to 60% in 5% increments) on the structure and optical properties. The main goal is to enhance the luminescence and color purity of yttrium borates by establishing a repeatable synthesis method, investigating structural changes as a result of varying composition, and minimizing the "parasitic" orange emission.

## 2. Materials and Methods

For the synthesis of photoluminescence yttrium borate $YBO_3$ doped with europium, the following reagents of analytical grade purity were used: $Y_2O_3$ (Yttrium (III) oxide, 99.99% (trace metal basis), CAS: 1314-36-9); $H_3BO_3$ (Boric acid, 99%, Index # 005-007022-2); Europium sulfate octahydrate $Eu(SO_4)_2.8H_2O$ (99.9%) purchased from Alfa Aesar(Thermo Fisher (Kandel) GmbH, Erlenbachweg 2, 76870 Kandel, Germany).

### *2.1. Sample Preparation*

The reagents were weighed, mixed, and homogenized. After that, the prepared mixtures were placed in alumina crucibles for the solid-state synthesis, and for the microwave-

assisted method, the samples were placed in Teflon sleeves and heated up. The sample contents are presented in Table 1.

The solid-state synthesis was performed in a muffle furnace at 1160 °C for 4 h with a heating rate of 15 °C/min. After 4 h, the samples were kept in the furnace, where they cooled slowly for 16 h. The sample S20 SS was prepared by mixing stoichiometric amounts of $Y_2O_3$ and $H_3BO_3$ with 2 mol% $Eu_2(SO_4)_3.8H_2O$ as a doping agent, as shown in Equation (6). In the samples from S21 SS to S212 SS, the content of $H_3BO_3$ excess rose from 5 mass% to 60 mass % with a step of 5 mass %. The samples in the series S20–S212 MW were synthesized by the microwave-assisted method using the same amounts of the starting substances obtained in a stoichiometric ratio, with the addition of 5 mL of distilled water. The synthesis temperature of the samples was 260 °C, the required time to reach the set temperature was 15 min, there was a hold of 10 min, and the cooling time was 20 min. The power of the microwave was 1500 watts. After cooling, the samples were removed dry.

$$Y_2O_3 + 2H_3BO_3 \rightarrow 2YBO_3 + 3H_2O \quad (6)$$

**Table 1.** Description of samples.

| Sample Code, Series SS | Sample Code, Series MW | Amount of $Y_2O_3$ (g) | Amount of $Eu(SO_4)_2.8H_2O$ (g) | $H_3BO_3$, g (% Excess) |
|---|---|---|---|---|
| S20 SS | S20 MW | 0.6446 | 0.1472 | 0.3537 (0%) |
| S21 SS | S21 MW | | | 0.3713 (5%) |
| S22 SS | S22 MW | | | 0.3891 (10%) |
| S23 SS | S23 MW | | | 0.4067 (15%) |
| S24 SS | S24 MW | | | 0.4244 (20%) |
| S25 SS | S25 MW | | | 0.4421 (25%) |
| S26 SS | S26 MW | | | 0.4598 (30%) |
| S27 SS | S27 MW | | | 0.4772 (35%) |
| S28 SS | S28 MW | | | 0.4949 (40%) |
| S29 SS | S29 MW | | | 0.5126 (45%) |
| S210 SS | S210 MW | | | 0.5303 (50%) |
| S211 SS | S211 MW | | | 0.5479 (55%) |
| S212 SS | S212 MW | | | 0.5656 (60%) |

## *2.2. Sample Analysis*

### 2.2.1. XRD Analysis

The crystal structure of synthesized phosphors was proven by X-ray diffraction (XRD, Siemens 500) with CuKa radiation (k = 1.54 A). The crystal structure was modeled using Crystalmaker software 10.6 (CrystalMaker Software Ltd., Oxford, UK; http://www.crystalmaker.com (accessed on 8 June 2024)). The lattice parameters were obtained by using MDI Jade version 9.1 the software (Material Data Inc., Livermore, CA, USA; http://www.materialsdata.com (accessed on 8 June 2024)).

### 2.2.2. FT-IR Analysis

The FT-IR spectra of the samples were recorded at a band sensitivity in the MIR 4000–400 $cm^{-1}$ region at a resolution of 2 $cm^{-1}$ in 25 scans using the FT-IR Bruker Vertex 70 Spectrometer. The samples for analysis were prepared in tablet form by thoroughly mixing 150 mg of KBr and 5 mg of the material (S 20–212 SS/MW) in a mortar. The mixture was thoroughly homogenized and subsequently compressed using a tablet press to form the final tablets.

### 2.2.3. Photoluminescent Analysis

The photoluminescence spectra were measured at room temperature using an Ocean Optics fiber-optic QEB1104 spectrometer in the range 200–990 nm and a combination of an energetic laser-driven white light source (190 nm–2500 nm) and a fiber-optic monochromator (MonoScan 2000, Ocean Optics) as illustrated in Figure 2. Large-core (1 mm) quartz

polymer fibers were used in the setup. The receiving fiber was placed at 45° with respect to the vertical excitation fiber. The main advantage of this scheme is that it minimizes reflection from the samples and maximizes the intensity of the luminescence spectra. The excitation wavelength was scanned from 220 nm to 550 nm at increments of 2 nm, and for each increment, we measured the fluorescence spectrum.

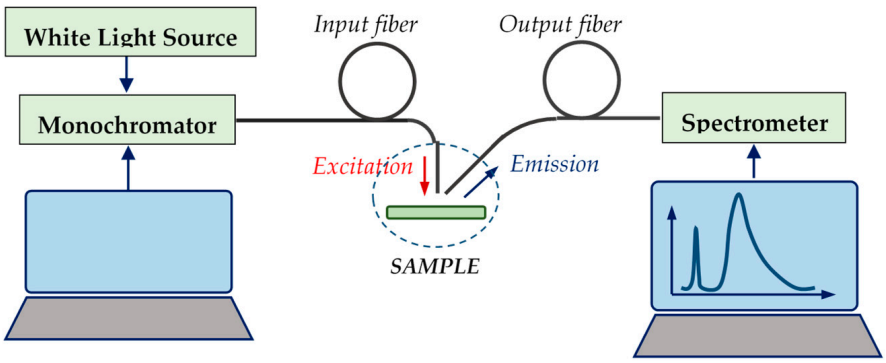


**Figure 2.** Scheme of the photoluminescent setup.

## 3. Results

### *3.1. Structural Characterization*

The prepared samples appeared as fine white powders. The X-ray diffraction data (Figure 3A) for the samples in the SS series show that those with 5% to 60% excess of boric acid have a vaterite-type structure with a hexagonal unit cell and a space group P63/m (JCPDF 16-0277) as described by Chadeyron et al. [17]. The most intense peaks from the X-ray diffraction patterns can be described by their 2θ positions and the corresponding hkl reflections: 20.1508 (002), 27.2483 (100), 29.1052 (101), 34.1245 (102), 40.9610 (004), 48.1569 (110), 49.8952 (104), 52.7078 (112), 60.3361 (202), and 65.0236 (114). No additional peaks were found in the X-ray diffraction (XRD) patterns of all the samples synthesized by the microwave-assisted method (see Figure 3B). The structure of $YBO_3$ generated from the software is shown in Figure 3C. The Y atoms are eight-fold coordinated by oxygen atoms ($YO_8$) in a trigonal bicapped antiprism polyhedron. Only the XRD data of the stoichiometric sample S20 show different peak positions characteristic of cubic $Y_2O_3$ (JCPDS 79-1257).

The transmission infrared (FTIR) spectra of the starting reagents and the samples were analyzed, and the observations are discussed below. An FTIR spectrum of boric acid (Figure 4) shows typical signals belonging to orthoboric acid [18]. The bands at 547, 647, 676, 792, 884, 1195, 1228 (shoulder), and 1470 $cm^{-1}$ belong to boric acid $H_3BO_3$. The band at 647 $cm^{-1}$ [19] is due to deformation vibrations of the atoms in the B–O bond. The slight broadening indicates the presence of no molecular water in the form of structure-forming OH groups. The band at 676 $cm^{-1}$ is assigned to vibrations of the $[BO_3]^{3-}$ structural group, the B–O–B bridge, or to vibrations of the atoms that form $[B(O, OH)_4]$ tetrahedrons [14,15]. The band at 1194 $cm^{-1}$ was probably caused by vibrations of atoms in the –O–B< bond in the structure of orthoboric acid. The bands at 2000, 2031, 2100, 2261, and 2361 $cm^{-1}$ could be caused by stretching vibrations of atoms in the C–O bond of gaseous $CO_2$ sorbed in the powder analyzed. The weak band at 2518 $cm^{-1}$ indicates molecular water impurity adsorbed on particles of the acid from the atmosphere. The next bands, including the band at 3222 $cm^{-1}$ with the highest peak height, belong to the water of a similar structural type but different from the preceding type. Medvedev et al. [18] found there are two forms of water.

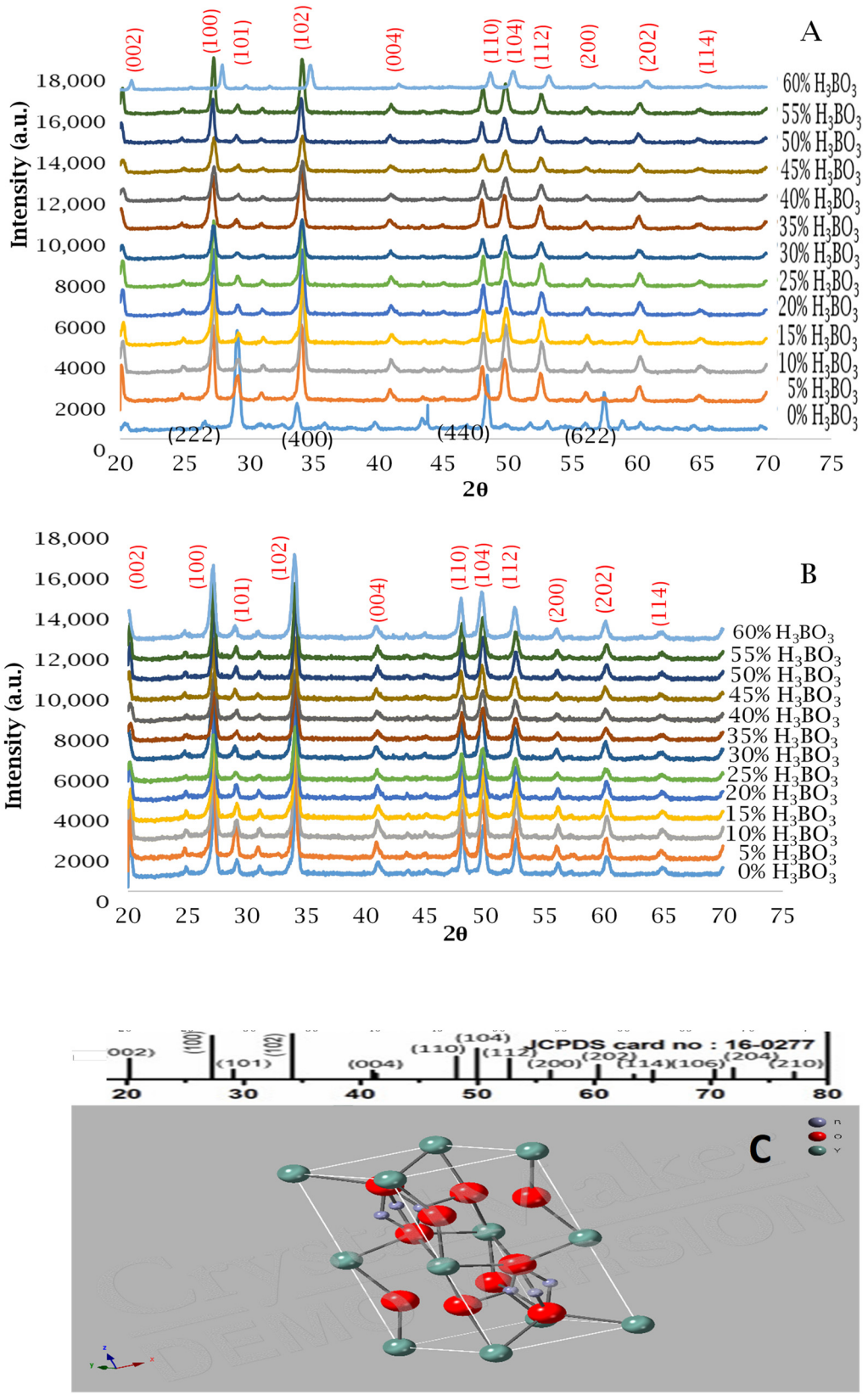


**Figure 3.** (**A**) XRD patterns of $YBO_3$:Eu samples (series SS) with increasing boric acid excess. (**B**) XRD patterns of $YBO_3$:Eu samples (series MW) with increasing boric acid excess. (**C**) Crystal structure of $YBO_3$.

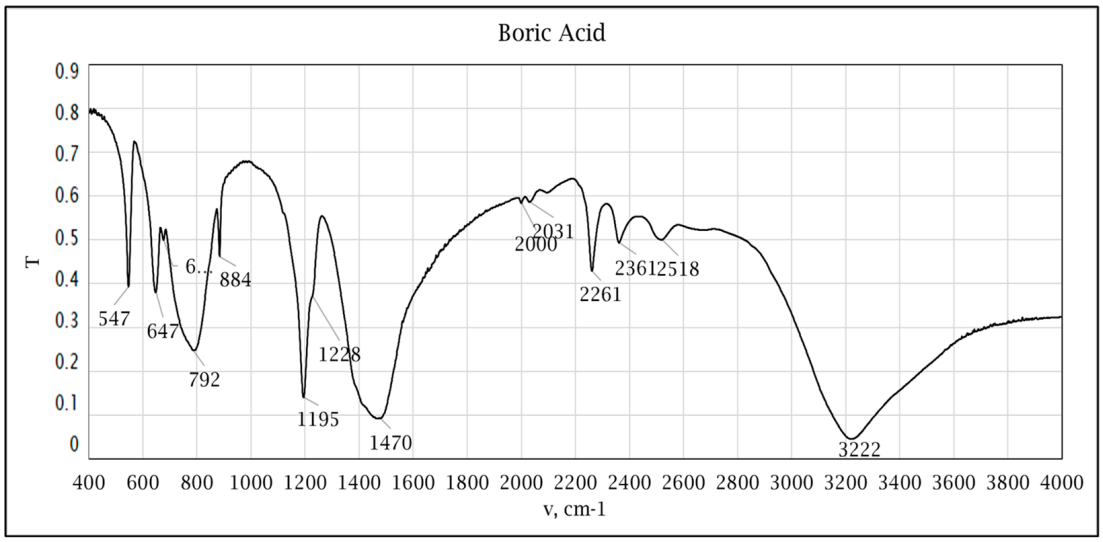


**Figure 4.** FTIR spectrum of boric acid used for starting raw material.

The infrared spectra of all samples of the SS series showed a structural modification with increasing boric acid excess. The stoichiometric sample S20 (Figure 5) shows bands at 1307 $cm^{-1}$ which are typical for isolated $[BO_3]^{3-}$ and for BO groups at about 1200 $cm^{-1}$, which is an indicator of the formation of a high-temperature $YBO_3$ phase with three-coordinated boron atoms. Examining the spectra of the starting materials and sample S20, we observe overlapping low-frequency bands corresponding to yttrium oxide located at 561 $cm^{-1}$ and 464 $cm^{-1}$ that are not present in the spectra of samples S21–S212 (Figure 6).

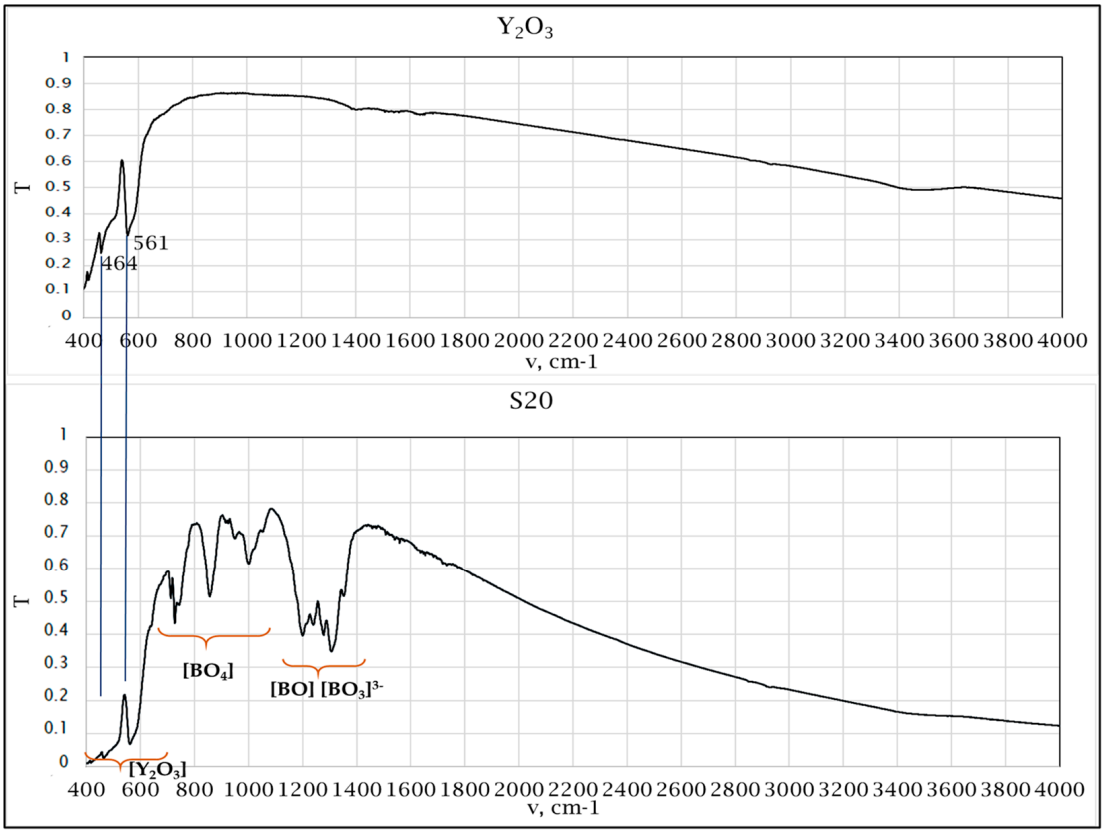


**Figure 5.** FTIR spectra of yttrium oxide and stoichiometric sample S20SS.

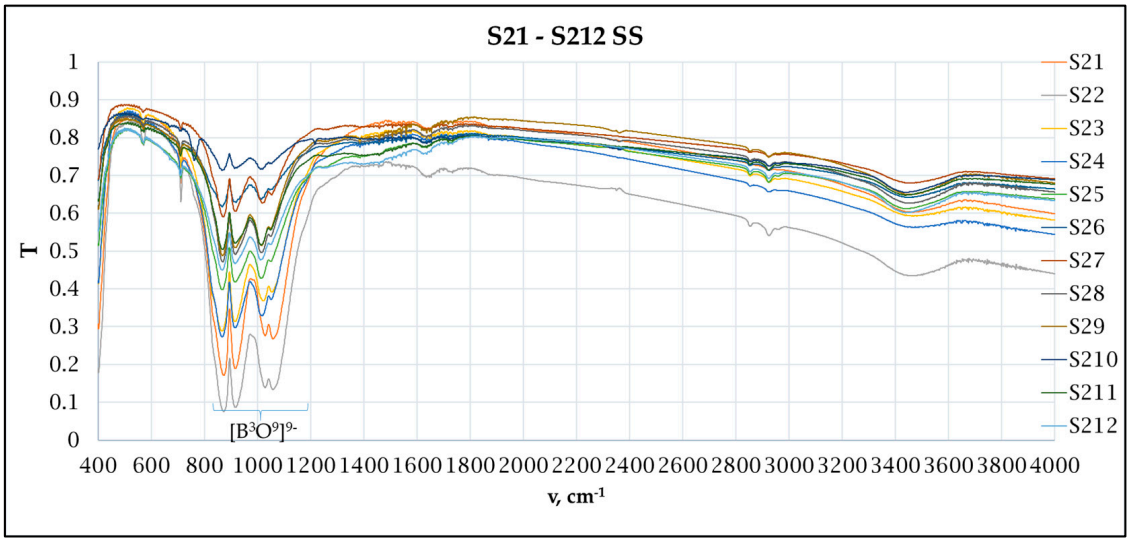


**Figure 6.** FTIR spectra of samples S21–S212 SS.

The infrared spectra of samples S21 SS to S212 SS overlap (Figure 6) and show no bands around 1300 $cm^{-1}$, which means that the $YBO_3$ phase includes only condensed borate groups linked together in the form of a boroxol ring $[B_3O_9]^-$. The phase transition from the low temperature (LT) to the high temperature (HT) phase is accompanied by the rupture of the boroxol ring, in which isolated borate groups $[BO_3]$ and [B–O] are located. Therefore, in the reversible process (HT–LT), isolated $[BO_3]$ groups condense to a boroxol ring $[B_3O_9]$.

For the samples synthesized by the microwave-assisted method, the IR spectrum of $YBO_3$:Eu has two well-defined band groups with doublet character (Figure 7), the first group with bands at 874 $cm^{-1}$ and 920 $cm^{-1}$, and the second group with bands at 1032 $cm^{-1}$ and 1075 $cm^{-1}$, similar to the bands reported in [19,20] and the same as those for series S2 SS. The spectrum with strong bands between around 862 and 1078 $cm^{-1}$ is clearly indicative of $[B_3O_9]^{9-}$ groups in $YBO_3$. The bands at 873 and 920 $cm^{-1}$ are due to ring stretching modes, whereas the peak at 1078 $cm^{-1}$ is due to terminal B-O stretching. The bending vibrations of the B–O–B bond in the borate network are located at ≈710 $cm^{-1}$. The strong band at ≈570 $cm^{-1}$ is attributed to Y-O in $Y_2O_3$ [21,22]. A broad peak at around 3217 $cm^{-1}$ originated from O–H stretching in hydroxyl groups [23]. All observed bands are described in Table 2.

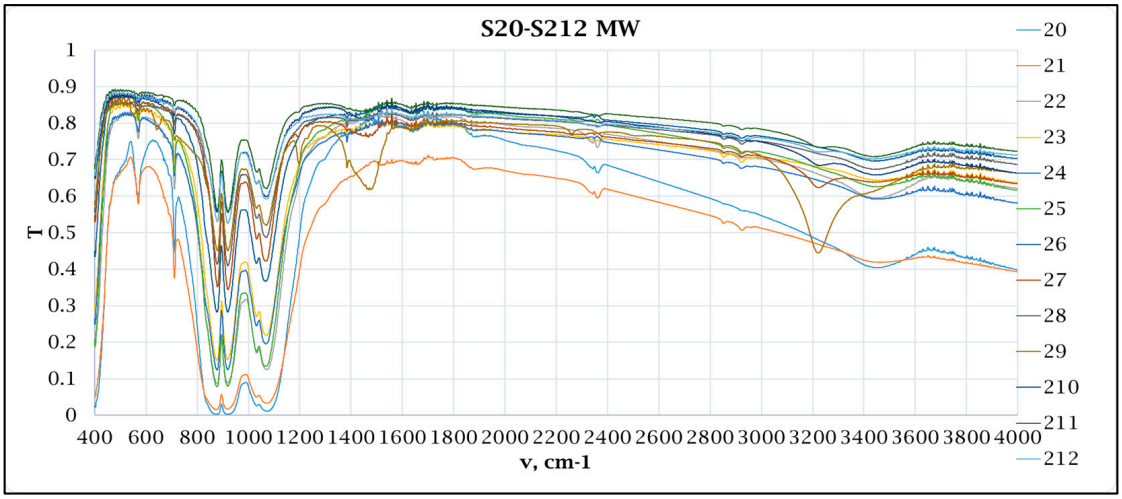


**Figure 7.** FTIR spectra of samples S20–212 MW with a variety of boric acid excess levels.

**Table 2.** Description of general bands present in FTIR spectra.

| Bands $cm^{-1}$ | Boric Acid | Yttrium Oxide | S20 | S0 MW |
|---|---|---|---|---|
| Y–O | | 464 | 464 | |
| δ([$BO_3$]–O)<br>δ(B–O), in-plane O–B–O angle deformation mode | 547 | | | |
| v (Y–O in $Y_2O_3$) | | 561 | 563 | |
| γ([$BO_3$]=O)<br>γ(O=H), out-of-plane OH deformation mode | 647<br>broadening | | | |
| $v_4$ ([$BO_3$]$^{3-}$) orv([B(O, OH)$_4$]) | 676 | | | |
| δ(B–O–B) | | | 711 | 711 |
| γ(B=O), out-of-plane $BO_3$ angle deformation mode<br>γ(O=H), twisting | 792 | | | |
| ring stretching | | | 873 | |
| ring stretching | | | | 878 |
| $v_s$(–O–B<) | 884 | | | |
| ring stretching | | | 916 | |
| ring stretching | | | | 919 |
| terminal B–O stretching | | | 1058 | |
| terminal B–O stretching | | | | 1069 |
| $v_{as}$([–O–B<]–O)<br>δ(O–H), in-plane B=O=H angle deformation mode | 1195 | | | |
| isolated [BO] | | | 1203 | |
| shoulder | 1225 | | | |
| isolated [$BO_3$]$^{3-}$ | | | 1307 | |
| $v_{as}$(–B–O) | 1470 | | | |
| No B–O modes (adsorbed gaseous $CO_2$), $B_2O_3$ impurities or combination frequencies of ν(O–H), ν(B–O), δ(O–H), δ(B–O) [24] | 2000 | | | |
| | 2031 | | | |
| | 2261 | | | |
| | 2361 | | | |
| ν(–O–H) from absorbed water | 2518 | | | |
| ν(–O–H) from water | 3222 | | | |

### *3.2. Photoluminescent Properties*

The fluorescence analysis performed with the setup from Figure 2 for the SS and MW samples revealed that for all samples, the highest fluorescence was observed at 260 nm (corresponding to $^7F_0 \rightarrow {}^5D_4$) and 396 nm ($^7F_0 \rightarrow {}^5L_6$) excitation wavelengths, the latter being the most efficient. For both the 260 nm and the 396 nm excitations, the emission spectra exhibited several peaks in the range from 590 nm to 800 nm, as shown in Figure 8a (for SS) and Figure 8b (for MW). These peaks were attributed to the transition of europium ions from the $^5D_0$ state to various $^7F_J$ (J = 0, 1, 2, 3, 4) levels.

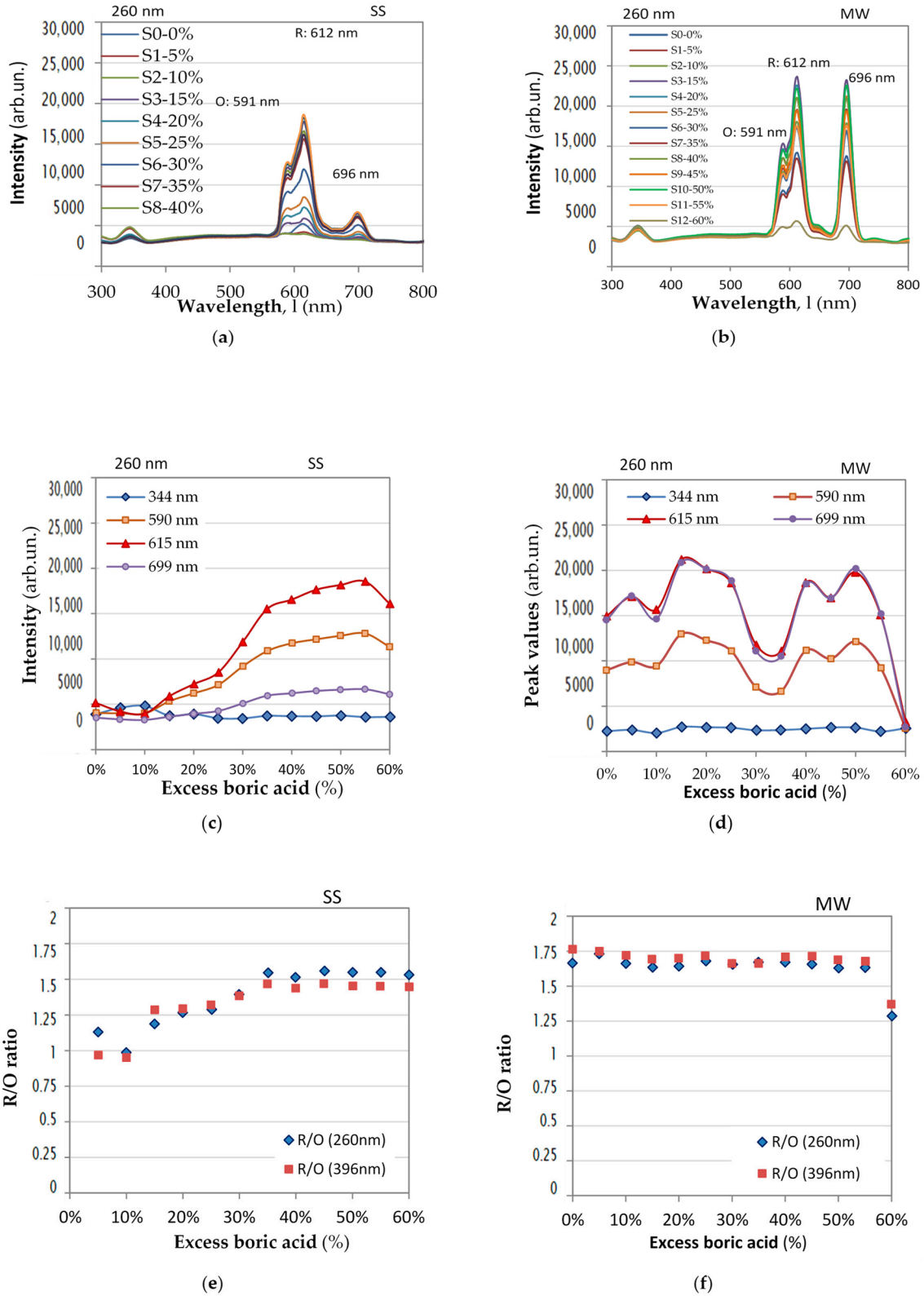


**Figure 8.** Comparison between SS and MW samples: (**a**,**b**) fluorescence spectra for different excess boric acid percentages; (**c**,**d**) intensities at four peak wavelengths for 260 nm excitation vs. percentage of excess boric acid; (**e**,**f**) dependences of the O/R ratios on the excess boric acid percentage for 260 and 396 nm excitations.

The following specific observations regarding the emission peaks can be outlined:

1. Orange emission ($^5D_0 \rightarrow {}^7F_1$): A peak at 591 nm was identified, corresponding to the $^5D_0 \rightarrow {}^7F_1$ transition, resulting in orange emission.
2. Red emission ($^5D_0 \rightarrow {}^7F_2$): Peaks at 612 nm and 620 nm were observed, corresponding to the $^5D_0 \rightarrow {}^7F_2$ transition, resulting in red emission.
3. Transition intensity and matrix influence:
   - When $Eu^{3+}$ ions occupy inversion center sites, the $^5D_0 \rightarrow {}^7F_1$ transitions were expected to be relatively strong, while the $^5D_0 \rightarrow {}^7F_2$ transitions were relatively weak.
   - The transition $^5D_0 \rightarrow {}^7F_1$ due to the magnetic dipole is independent of the host matrix, whereas the $^5D_0 \rightarrow {}^7F_2$ transition allowed by the electric dipole is strongly influenced by the local structure.
4. Emission intensity ratio (R/O Ratio):
   - The emission intensity ratio between red and orange color transitions, denoted as R/O ($I(^5D_0 \rightarrow {}^7F_2)/I(^5D_0 \rightarrow {}^7F_1)$), was calculated by considering the sum of the integral intensities of the red emission peak observed at 612 nm for the contribution of the $^5D_0/{}^7F_2$ transition. The intensities of the different $^5D_0$–$^7F_J$ transitions and the splitting of these emission peaks depend on the local symmetry of the crystal field of the $Eu^{3+}$ ion. If the $Eu^{3+}$ ion occupies a centrosymmetric site in the crystal lattice, the magnetic dipole transition $^5D_0$–$^7F_1$ (orange) is the dominant transition; otherwise, the electric dipole transition $^5D_0$–$^7F_2$ (red) becomes dominant.
   - This ratio, also known as the asymmetric ratio, color purity, or red-to-orange emission ratio, provides insights into the relative strengths of the red and orange emissions. $YBO_3$:$Eu^{3+}$ has a hexagonal structure of the vaterite type, with $Eu^{3+}$ ions occupying the $Y^{3+}$ site, which has point symmetry S 6. As a result, the orange emission at 592 nm from the $^5D_0 = {}^7F_1$ transition is dominant, leading to a lower value of the intensity ratio (R/O) between red and orange emission. Good color purity requires a high R/O value, and thus, many studies aim to improve this ratio.
5. Emission at 696 nm corresponds to the $^5D_0 \rightarrow {}^7F_4$ electronic transition whose intensity is comparable to that of the 612 nm peak for 396 nm excitation and considerably lower for 260 nm excitation.

In Figure 8c,d, we show the dependence of the peak values at these specific wavelengths on the percentage of the excess boric acid for the SS and MW samples correspondingly for 260 nm excitation.

## 4. Discussion

The X-ray structural analysis confirms the formation of a crystalline structure described as yttrium borate in most samples. An exception is the stoichiometric sample obtained by the solid-phase method whose X-ray data well describe the structure of yttrium oxide. The data shown in Figure 3A reveal changes in the intensity of the main peaks, indicating variations in the crystallinity of the materials due to increasing boric acid content. Sample 212SS (60% boric acid) shows a shift in the positions of the main peaks towards larger angles, along with broader and diffuse peaks instead of narrow and sharp. Furthermore, the intensity of the peaks decreases significantly in this sample, suggesting that this represents the upper limit of boric acid content. As is known, $H_3BO_3$ acts as a flux material, and the use of small amounts of this additive improves the crystallinity of synthesized phosphorus. This is because small amounts of $H_3BO_3$, with a relatively lower melting point, act as a flux and enhance the growth of yttrium crystals. However, higher amounts of $H_3BO_3$ not only decrease the peak intensity but also shrink the interplanar distance, in similar work from 3.059 to 3.053 and 3.052 Å [25]. This observation reveals that relatively larger amounts of $H_3BO_3$ suppress the growth of $YBO_3$. The boron oxide formed as a result

of the high synthesis temperature and the excessive excess of the raw material probably starts the formation of an amorphous structure. It is clear from the X-ray data of the MW series that the formation of the desired phase was achieved without the influence of boric acid. In all MW samples, the main peak positions match well with the structure generated in Figure 3C.

FTIR spectra of samples in the solid-state series show structural modifications with increasing boric acid excess. The stoichiometric sample S20 SS shows bands indicating the formation of a high-temperature $YBO_3$ phase. Samples S21 SS to S212 SS show no bands around 1300 $cm^{-1}$, suggesting that the $YBO_3$ phase includes only fused borate groups linked in a boroxol ring $[B_3O_9]^-$. Increasing boric acid, even in small excess, led to a compaction of the structure and the formation of a low-temperature phase (LT) where boron is four-coordinated.

All samples synthesized by the microwave-assisted method showed the formation of boroxol rings, regardless of the excess amount of boric acid. The strong band observed at approximately 570 $cm^{-1}$ is attributed to Y–O in $Y_2O_3$. In addition, a broad peak at around 3217 $cm^{-1}$ is observed, which is due to the O–H stretching of hydroxyl groups as a result of the residual amounts of absorbed water. This issue can be solved by applying additional drying after the synthesis process.

Fluorescence analysis highlights the excitation wavelengths and emission transitions of europium ions in the synthesized samples.

As seen in Figure 8, the main difference between the two types of samples is in the strength of the 696 nm emission, which is comparable to the orange emission at 612 nm for the MW samples and significantly lower for the SS samples. The second difference is that the fluorescence intensity of the MW series is higher compared to that of the SS series. The dependencies for 396 nm excitation are similar.

Figure 8e,f show the dependence of the O/R ratio on the percentage of excess boric acid for 260 nm and 396 nm UV excitation. From these figures, it is evident that for the SS samples, the O/R ratio increases with the excess boric acid, reaching a saturation level of about 1.5 above 35%, while for the MW samples, it remains practically constant at 1.7–1.75 levels and is slightly higher for 396 nm excitation. For all samples, the fluorescence strongly diminishes above 60% excess boric acid. As we see, unlike the fluorescence intensity and spectral distributions (Figure 8a,b), the O/R ratios are weakly affected by the excitation wavelength. They, however, depend on the type of samples i.e., on the technology—solid-state vs. microwave-assisted. The latter is characterized by a stronger fluorescence and a higher O/R ratio. The enhanced red emission of $YBO_3$:Eu synthesized by the microwave-assisted method compared to samples obtained by the solid-state reaction is due to better structural substitution of europium ions for yttrium ions [26,27].

In view of the above observations, the second group of MW samples produced by the microwave-assisted method is more suitable for smartphone-readable markers. The observed orange and red emissions, along with the calculated R/O ratio, contribute to the understanding of the luminescent properties of the materials. These properties are crucial for potential applications in areas such as optoelectronics, displays, and luminescent devices [28,29].

## 5. Conclusions

In summary, we report a study on the influence of boric acid content and synthesis conditions on the structural features and photoluminescence properties of the target yttrium borate. Two series of samples with variable excess boric acid from 5% to 60% synthesized by two different methods are presented.

Structural and fluorescence analyses elucidate the influence of the synthesis method and excess boric acid on the properties of the $YBO_3$ materials. Microwave-assisted synthesis consistently yields samples with boroxol ring formations and improved fluorescence properties compared to the solid-state method. Increasing excess boric acid can cause structural changes depending on the synthesis method. Its presence is known to improve

the crystallinity of materials. The emission intensity increases linearly and exponentially with increasing boric acid content in the samples synthesized by solid-phase reaction, while no such dependence is observed in those synthesized by microwave technology. In the samples synthesized by microwave technology, a significant increase in intensity and enhancement of the red emission was observed, probably caused by a better substitution of the yttrium ions by the doping agent. This substitution indicates that the europium ions are more uniformly and more fully integrated into the crystal structure, leading to improved fluorescence properties of the material. Microwave synthesis can facilitate faster heating, which favors a more efficient replacement of yttrium ions with europium ions. This can lead to better distribution and fewer defects in the crystal structure, which in turn enhances the red emission. All of these observations provide a good correlation between structure and properties. These findings highlight the importance of synthesis parameters in tailoring the luminescence properties of materials for specific applications, with microwave probes showing promise for applications requiring strong fluorescence and consistent performance under varying synthesis conditions.

**Author Contributions:** Conceptualization, I.P.K. and T.A.E.; methodology, S.N., A.P. and K.H.; software, T.A.E. and S.T.; validation, S.N., S.T. and A.P.; formal analysis, K.H.; investigation, I.P.K.; resources, I.P.K. and T.A.E.; data curation, T.A.E.; writing—original draft preparation, I.P.K. and T.A.E.; writing—review and editing, K.H.; visualization, K.H.; supervision, I.P.K.; project administration, T.A.E.; funding acquisition, I.P.K. All authors have read and agreed to the published version of the manuscript.

**Funding:** This research was funded by the Natural Sciences and Engineering Council (NSERC), Canada under Discovery grant DDG-2021-00022.

**Data Availability Statement:** The raw data supporting the conclusions of this article will be made available by the authors on request.

**Conflicts of Interest:** The authors declare no conflicts of interest.

## References

1. Plewa, J.; Jüstel, T. Phase transition of $YBO_3$. *J. Therm. Anal. Calorim.* **2007**, *88*, 531–535. [CrossRef]
2. Fuchs, B.; Schröder, F.; Heymann, G.; Siegel, R.; Senker, J.; Jüstel, T.; Huppertz, H. Crystal structure re-determination, spectroscopy, and photoluminescence of $\pi$-$YBO_3$:$Eu^{3+}$. *Z. Anorg. Allg. Chem.* **2021**, *647*, 2035–2046. [CrossRef]
3. Sevim, F.; Demir, F.; Bilen, M.; Okur, H. Kinetic analysis of thermal decomposition of boric acid from thermogravimetric data. *Korean J. Chem. Eng.* **2006**, *23*, 736–740. [CrossRef]
4. Harabor, A.; Rotaru, P.; Scorei, R.I.; Harabor, N.A. Non-conventional hexagonal structure for boric acid. *J. Therm. Anal. Calorim.* **2014**, *118*, 1375–1384. [CrossRef]
5. Huber, C.; Jahromy, S.S.; Birkelbach, F.; Weber, J.; Jordan, C.; Schreiner, M.; Harasek, M.; Winter, F. The multistep decomposition of boric acid. *Energy Sci. Eng.* **2020**, *8*, 1650–1666. [CrossRef]
6. Ben Smida, Y.; Marzouki, R.; Kaya, S.; Erkan, S.; Faouzi Zid, M.; Hichem Hamzaoui, A. Synthesis Methods in Solid-State Chemistry. In *Synthesis Methods and Crystallization*; Marzouki, R., Ed.; InTech Open: London, UK, 2020; pp. 1–13. [CrossRef]
7. Kitchen, H.J.; Vallance, S.R.; Kennedy, J.L.; Tapia-Ruiz, N.; Carassiti, L.; Harrison, A.; Gregory, D.H. Modern Microwave Methods in Solid-State Inorganic Materials Chemistry: From Fundamentals to Manufacturing. *Chem. Rev.* **2013**, *114*, 1170–1206. [CrossRef] [PubMed]
8. Liu, F.W.; Hsu, C.H.; Chen, F.S.; Lu, C.H. Microwave-assisted solvothermal preparation and photoluminescence properties of $Y_2O_3$:$Eu^{3+}$ phosphors. *Ceram. Int.* **2012**, *38*, 1577–1584. [CrossRef]
9. Boyer, D.; Bertrand-Chadeyron, G.; Mahiou, R.; Brioude, A.; Mugnier, J. Synthesis and characterization of sol–gel derived $Y_3BO_6$:$Eu^{3+}$ powders and films. *Opt. Mater.* **2003**, *24*, 35–41. [CrossRef]
10. Maia, L.J.Q.; Mastelaro, V.R.; Pairis, S.; Hernandes, A.C.; Ibanez, A. A sol–gel route for the development of rare-earth aluminum borate nanopowders and transparent thin films. *J. Solid State Chem.* **2007**, *180*, 611–618. [CrossRef]
11. Gangwar, A.K.; Nagpal, K.; Kumar, P.; Singh, N.; Gupta, B.K. New insight into printable europium-doped yttrium borate luminescent pigment for security ink applications. *J. Appl. Phys.* **2019**, *125*, 074903. [CrossRef]
12. Zhang, X.; Fu, Y.; Zhao, Z.; Yang, J.; Li, N.; Zhang, M. Statistical design for the optimization of the red to orange ratio in $YBO_3$:$Eu^{3+}$ phosphors. *J. Lumin.* **2018**, *194*, 311–315. [CrossRef]
13. Novotný, M.; Remsa, J.; Havlová, Š.; More-Chevalier, J.; Irimiciuc, S.A.; Chertopalov, S.; Písařík, P.; Volfová, L.; Fitl, P.; Kmječ, T.; et al. In Situ Monitoring of Pulsed Laser Annealing of Eu-Doped Oxide Thin Films. *Materials* **2021**, *14*, 7576. [CrossRef]

14. Nayak, B.B.; Srivastava, S.; Singh, A.K.; Behera, S.K. Influence of high energy milling on powder morphology and photoluminescence behavior of Eu-doped $YBO_3$ material. *Mater. Chem. Phys.* **2020**, *254*, 123429. [CrossRef]
15. Rafiaei, S. The luminescence properties of yttria based phosphors and study of $YBO_3$ formation via $H_3BO_3$ addition. *Process. Appl. Ceram.* **2018**, *12*, 262–267. [CrossRef]
16. Rafiaei, S.M.; Kim, A.; Shokouhimehr, M. Enhanced luminescence properties of combustion synthesized $Y_2O_3$:Gd nanostructure. *Current. Nanosci.* **2016**, *12*, 244–249. [CrossRef]
17. Chadeyron, G.; El-Ghozzi, M.; Mahiou, R.; Arbus, A.; Cousseins, J.C. Revised Structure of the Orthoborate $YBO_3$. *J. Solid State Chem.* **1997**, *128*, 261. [CrossRef]
18. Medvedev, E.F.; Komarevskaya, A.S. IR spectroscopic study of the phase composition of boric acid as a component of glass batch. *Glass Ceram.* **2007**, *64*, 42–46. [CrossRef]
19. Vlasov, A.G.; Florinskaya, V.A. (Eds.) *Structure and Physicochemical Properties of Inorganic Glasses*; Khimiya: Leningrad, Russia, 1974. (In Russian)
20. Kazuo, N. Infrared and Raman Spectra of Inorganic and Coordination Compounds. In *Theory and Applications in Inorganic Chemistry*, 6th ed.; Wiley: New York, NY, USA, 1997.
21. Stefanovskii, S.V.; Ivanov, I.A.; Gulin, A.N. IR and EPR spectra of aluminoborosilicate and aluminophosphate glasses simulating vitrified radioactive wastes. *Fiz. Khim. Stekla* **1991**, *17*, 120–125.
22. Beregi, E.; Watterich, A.; Kovács, L.; Madarász, J. Solid-state reactions in $Y_2O_3$:3$Al_2O_3$:4$B_2O_3$ system studied by FTIR spectroscopy and X-ray diffraction. *Vib. Spectrosc.* **2000**, *22*, 169–173. [CrossRef]
23. Onani, M.O.; Okil, J.O.; Dejene, F.B. Solution–combustion synthesis and photoluminescence properties of $YBO_3$:$Tb^{3+}$ phosphor powders. *Phys. B Condens. Matter* **2014**, *439*, 133–136. [CrossRef]
24. Schott, J.; Kretzschmar, J.; Acker, M.; Eidner, S.; Kumke, M.; Drobot, B.; Barkleit, A.; Taut, S.; Brendlera, V.; Stumpfa, T. Formation of a Eu(III) borate solid species from a weak Eu(III) borate complex in aqueous solution. *Dalton Trans.* **2014**, *43*, 11516. [CrossRef] [PubMed]
25. Miranda de Carvalho, J.; Pedroso, C.C.S.; Saula, M.S.d.N.; Felinto, M.C.F.C.; Brito, H.F.d. Microwave-Assisted Preparation of Luminescent Inorganic Materials: A Fast Route to Light Conversion and Storage Phosphors. *Molecules* **2021**, *26*, 2882. [CrossRef] [PubMed]
26. Nazarov, M.V.; Kang, J.H.; Jeon, D.Y.; Popovici, E.J.; Muresan, L.; Tsukerblat, B.S. Lattice parameter and luminescence properties of europium activated yttrium oxide. *Solid State Commun.* **2005**, *133*, 183–186. [CrossRef]
27. Anitha, M.; Mohapatra, M.; Kadam, R.M.; Seshagiri, T.K.; Tyagi, A.K.; Natarajan, V. Thermally stimulated luminescence and electron paramagnetic resonance studies of $Eu^{3+}$-doped yttrium borate. *J. Mater. Res.* **2006**, *21*, 1117–1123. [CrossRef]
28. Zhang, F.; Bian, G.; Ding, H.; Tang, J.; Li, X.; Zhang, C.; Li, S.; Jia, G. Controllable synthesis and tunable luminescence of yttrium orthoborate microcrystals with multiform morphologies and dimensions. *J. Lumin.* **2020**, *219*, 116890. [CrossRef]
29. Hristova, K.; Kostova, I.P.; Eftimov, T.A.; Brabant, D.; Fouzar, S. Rare-Earth-Ion ($RE^{3+}$)-Doped Aluminum and Lanthanum Borates for Mobile-Phone-Interrogated Luminescent Markers. *Photonics* **2024**, *11*, 434. [CrossRef]